Mapping Orientational Order of Charge-Probed Domains in a Semiconducting Polymer

Nicola Martino,[†,‡] Daniele Fazzi,[†,§] Calogero Sciascia,[†] Alessandro Luzio,[†] Maria Rosa Antognazza,[†] and Mario Caironi[†,*]

[†]Center for Nano Science and Technology @PoliMi, Istituto Italiano di Tecnologia, Via G. Pascoli 70/3, 20133 Milano, Italy, [‡]Dipartimento di Fisica, Politecnico di Milano, Piazza L. da Vinci, 32, 20133 Milano, Italy, and [§]Max-Planck-Institut für Kohlenforschung (MPI-KOFO), Kaiser-Wilhelm-Platz 1, D-45470, Mülheim an der Ruhr, Germany

ABSTRACT

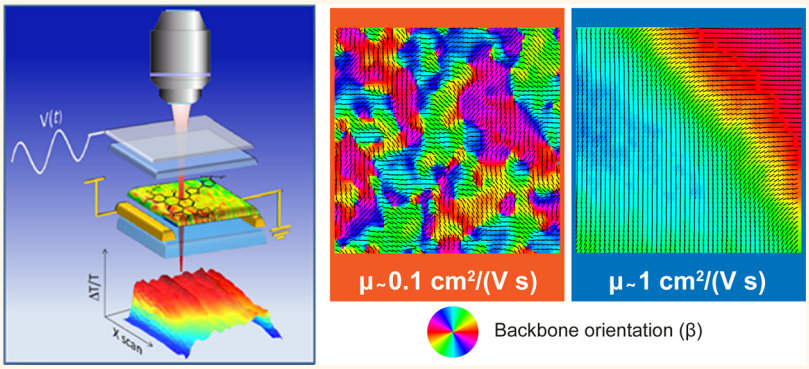

Structure—property relationships are of fundamental importance to develop quantitative models describing charge transport in organic semiconductor based electronic devices, which are among the best candidates for future portable and lightweight electronic applications. While microstructural investigations, such as those based on X-rays, electron microscopy, or polarized optical probes, provide necessary information for the rationalization of transport in macromolecular solids, a general model predicting how charge accommodates within structural maps is not yet available. Therefore, techniques capable of directly monitoring how charge is distributed when injected into a polymer film and how it correlates to structural domains can help fill this gap. Supported by density functional theory calculations, here we show that polarized charge modulation microscopy (p-CMM) can unambiguously and selectively map the orientational order of the only conjugated segments that are probed by mobile charge in the few nanometer thick accumulation layer of a high-mobility polymer-based field-effect transistor . Depending on the specific solvent-induced microstructure within the accumulation layer, we show that p-CMM can image charge-probed domains that extend from submicrometer to tens of micrometers size, with markedly different degrees of alignment. Wider and more ordered p-CMM domains are associated with improved carrier mobility, as extracted from device characteristics. This observation evidences the unprecedented opportunity to correlate, directly in a working device, electronic properties with structural information on those conjugated segments involved in charge transport at the buried semiconductor—dielectric interface of a field-effect device.

KEYWORDS: charge transport · organic transistor · polymer semiconductor · thin film microstructure · charge modulation spectroscopy

Semiconducting π-conjugated polymers are being extensively studied to unveil structure—property relationships,[1−5] which dictate their performances in optoelectronic devices. These fundamental studies have supported in the recent past the development of polymer-based organic field-effect transistors (OFET) with charge carrier mobility in the range from 1 to 10 $cm^2/(V\ s)$.[6−10] Such mobility values, although still inferior to inorganic semiconductor technologies, have been achieved with solution-processable semiconductors, which are enabling cost-effective printing techniques as fabrication tools for future generation large-area and flexible electronics products.[11,12]

Charge transport in polymeric materials is greatly influenced by morphological

* Address correspondence to mario.caironi@iit.it.

Received for review February 25, 2014 and accepted May 11, 2014.

Published online May 12, 2014
10.1021/nn5011182

properties at different length scales. Historically, semicrystalline molecular packing on the nanometre scale has been intensively investigated as the key to improve charge transport, owing to the efficient charge transfer path along the $\pi-\pi$ stacking direction.[13−15] The paradigm directly correlating charge mobility to the degree of crystallinity has however been recently challenged by a novel generation of donor−acceptor copolymers that, despite apparently lacking markedly crystalline order, present high charge mobilities.[16−20] Recent works highlighted the important role played by a more rigid backbone with respect to homopolymers[21] in locking microstructures characterized by long-range orientational order, extending to the micrometer scale,[22−24] and by a high degree of interconnectivity of more ordered domains through tie-molecules.[1,3] This complex structure is believed to compensate an overall limited degree of crystallinity by providing less sensitivity to morphological disorder.[1,25]

These structural features in semiconducting polymers have been mainly studied with techniques based on polarized electromagnetic radiation, both in the optical[26−29] and in the soft X-ray range.[1,22−24] These techniques can provide fundamental information on the microstructure of the material with very good spatial resolution (down to tens of nanometers in the case of X-ray radiation), can attain surface sensitivity,[30,31] and have allowed unveiling an important role of noncrystalline order.[1,22,23,27] However, the information they convey is purely morphological, and its correlation with the density of states involved in charge transport is not trivial, due to the current lack of a general enough transport model.

In the case of an OFET, which besides deserving technological interest is largely adopted as an investigation tool for the characterization of charge transport, mobile charge is transported in a few nanometers thick accumulation layer at the interface with the insulating layer. Transport properties are known to be affected by the polarizability of the dielectric[32,33] and by the physical interface formed between this and the semiconductor, a critical aspect in solution-based processes.[34] Moreover, at typical densities achieved in OFETs (usually from 10^{18} to a few 10^{19} cm^{-3}) the charge probes only up to 1% of all available electronic sites within the accumulation layer[35,36] (Supporting Information, Charge Density Estimation).

Techniques capable of providing selective structural information on the molecules actually hosting the charge at the buried interface in an OFET channel would therefore greatly expand the tools available to investigate structure−function relationships in polymeric semiconducting thin films.[37,38]

RESULTS

Charge modulation spectroscopy (CMS) is a powerful technique to study the semiconductor electronic states in a working transistor, probing the optical transitions induced by charge injected into the device.[39−41] We recently demonstrated that it is possible to couple this technique to a confocal microscope in order to obtain local CMS data with a submicrometer spatial resolution,[42] thus resulting in charge modulation microscopy (CMM). Here we demonstrate that by precisely controlling the polarization of the probe light, the distribution of the charged-induced features can be unambiguously related to structural properties as the local preferential alignment of the polymer conjugated segments. By simultaneously mapping the optical density (OD) of the film and the CMS signal, in combination with quantum-chemical calculations, we can provide information on the local alignment and degree of orientational order both of the bulk of the film and of the polymeric segments actually involved in the charge transport process in the accumulation layer. In this context, we introduce the concept of charge-probed (orientational) domains to refer to the domains arising in the CMS maps, which are composed only by the fraction of polymeric chains where charges reside at the interface with the dielectric. They are to be distinguished from the "standard" orientational domains usually probed by other techniques (and our OD signal), which are sensitive to all the molecules in the investigated volume, irrespectively of their involvement in transport.

We prove the potential of polarized CMM (p-CMM) in investigating structure−property relationships by comparing charge-probed domain dimensions and degree of orientation as measured on devices where charge carrier mobility was modulated by depositing the same polymer from different solvents. We neatly verify that a higher mobility is associated with a markedly larger extent of the charge-probed domains, exceeding the channel length, and with an improved degree of order.

Polarized Charge Modulation Microscopy. Since it is at the basis of the technique here presented and of the understanding of the experimental results, we recall the fundamentals of charge modulation microscopy, which we presented in a previous work,[42] demonstrating that it can be used to image the charge density profile along the channel of an OFET. CMM can be operated on complete and functioning devices (in this case a field-effect transistor, but it can be used also on other architectures such as metal−insulator−semiconductor structures[43]), where charge density is periodically varied by applying a modulated voltage to the gate electrode. A probe light beam (Supporting Information, Figure S1) is focused on the sample, and its transmission represents the collected signal, characterized by two components: (i) a dc component, which is related to the optical absorption of the ground state polymer and from which the optical density of the entire semiconducting layer can be extracted; (ii) an ac

component at the same frequency as the gate voltage related to the absorption of the probe beam by the accumulated charge. The latter component is thus arising only from those polymeric segments where charge is present, and it can be used to calculate what in the following we refer to as CMS signal (Supporting Information, Signal Measured by p-CMM). Spatial maps of these two signals (OD and CMS) are then reconstructed by raster scanning the sample.

Here we largely extend the capabilities of CMM thanks to two main improvements. The first regards the possibility to collect full local CMS spectra in the visible/near-infrared region thanks to the adoption of a supercontinuum white light laser as the probe light source. The second, enabled by the possibility to precisely control the probe polarization state, regards the detection of the dichroism in the collected signals. The dichroism can be correlated to anisotropies in the neutral and charge-induced absorption cross-section and, in turn, with the help of quantum-chemical calculations, to the molecular orientation.

We can thus retrieve morphological information on the material by mapping the optical signals of OD and CMS. However, while the two signals are collected simultaneously, they provide two very different pieces of information. From OD maps we can extract the orientation of polymeric backbones in the bulk of the film, which is what is usually done in polarized microscopy (in both the optical and X-ray regimes). On the other hand, from the CMS signal what we obtain is the morphological structure of only those polymeric segments hosting the injected charge. A cartoon depicting the different origin of the two signals from the probed region of the device is reported in Figure 1.

p-CMM Imaging on a P(NDI2OD-T2) Device. The devices investigated in this work (Supporting Information, Figure S2) are bottom-contact top-gate FETs based on the well-known n-type semiconductor poly{[*N*,*N*′-bis(2-octyldodecyl)-1,4,5,8-naphthalenedicarboximide-2,6-diyl]-*alt*-5,5′-(2,2′-bithiophene)} (indicated in the following as P(NDI2OD-T2)), which shows electron mobility that can exceed 1 $cm^2/(V\ s)$, depending on the deposition strategies adopted.[27] We first report on a transistor in which the semiconducting layer was deposited from a dichlorobenzene solution. The mobility extracted from the transfer characteristic curves of the device (Supporting Information, Figure S2) is 0.1 $cm^2/(V\ s)$, a typical value for the solvent adopted.[16]

Two OD maps, of a 10 × 10 μm^2 portion of the channel of the device, collected at λ = 690 nm (the maximum of P(NDI2OD-T2) absorption in the visible, Supporting Information Figure S3) with mutual-orthogonal polarizations, are reported in Figure 2a,b. The two maps are complementary, in the sense that higher transmission areas in Figure 1a correspond with lower transmission areas in Figure 2b and *vice versa*,

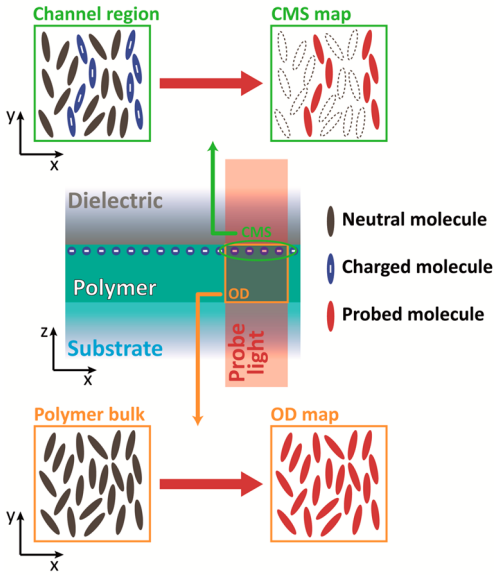

Figure 1. Scheme of a portion of the transistor probed by the laser light in a typical p-CMM measure. The bulk of the polymer, which gives the OD signal, is composed of neutral molecules that are indifferently probed by the light beam. On the other hand, at the interface with the dielectric, charges are accumulated due to the gate voltage modulation. Among all the molecules in this region, however, only a small fraction is charged (less than 1%); the CMS signal arises only from these charged molecules and is insensitive to the neutral ones. Note that the laser probe light, propagating along the *z*-axis, is polarized linearly in the *x*−*y* plane.

evidencing a preferential alignment of the transition dipole moments (TDMs) related to the electronic transition of the neutral species of P(NDI2OD-T2) (*i.e.*, $S_0 \rightarrow S_1$ transition). Figure 2c shows a typical profile of the OD signal *versus* the laser polarization (θ), with the data clearly following the theoretical $\cos^2(\theta)$ relationship. The limited depth of the signal modulation indicates however that a large fraction of the material has an isotropic absorption. These maps show similar trends to those previously reported by X-ray analysis[42] and represent morphological information on the TDM orientations averaged on the entire thickness of the semiconducting film.

The simultaneously collected CMS signal maps are plotted in Figure 2d,e. Due to the relatively high gate modulation frequency, the contribution to the signal comes only from the mobile polarons and not from deeply trapped charges[42] (Supporting Information Figure S4). The CMS signal thus provides selective information on the distribution of those states directly involved in determining the charge carrier mobility. It is worth noting that when probing the bleaching signal, we are still observing the TDM of the $S_0 \rightarrow S_1$ transition. The two CMS maps show as well a dichroic behavior, thus suggesting the presence of accumulation layer domains featuring a certain degree of preferential orientations of the TDMs. The modulation of the CMS signal by varying the probe polarization is however generally much higher (Figure 2f) with respect to what

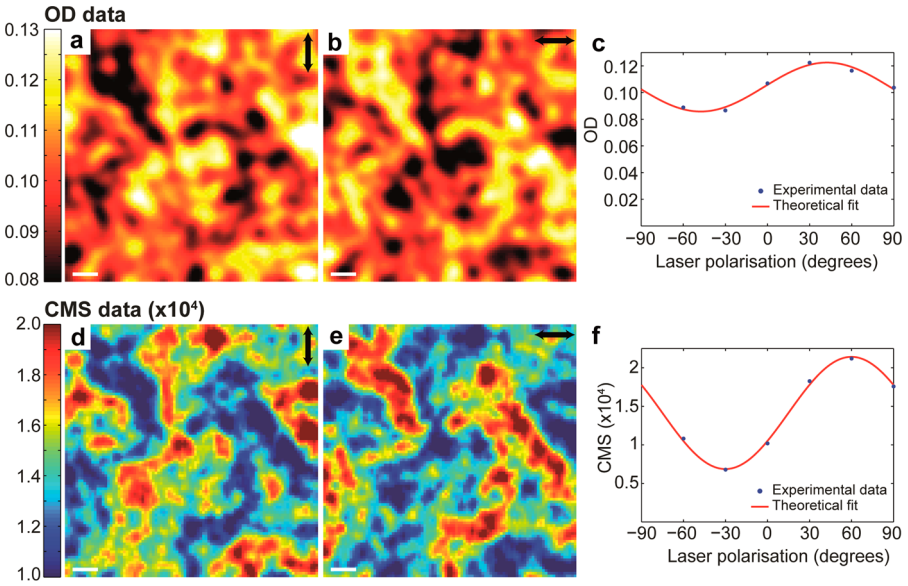

Figure 2. Polarized CMM maps of the channel of a P(NDI2OD-T2) transistor. (a, b) Optical density (OD, at $\lambda = 690$ nm) maps of a $10 \times 10\ \mu m^2$ area in the channel of the transistor taken with two orthogonal probe light polarizations. Scale bar is 1 μm. (c) Polarization dependence of the measured OD signal in a fixed point of the map, fitted to the expected $\cos^2(\theta)$ relation. (d, e) CMS (*i.e.*, the differential transmission $\Delta T/T$) maps of the same area as (a) and (b) taken at $\lambda = 690$ nm with the same two orthogonal. (f) Angular dependence (experimental data and fitting) of the differential transmission signal taken at the same point as (c).

is observed in the OD maps. It is also to be noted that the features appearing in the CMS maps correlate quite nicely to those in the relative OD images.

Local CMS Spectra. While the results reported in Figure 2 are evidence of the presence of charge-probed domains featuring a preferential alignment of the TDM of the neutral polymer segments, it cannot be excluded that part of the observed spatial modulation of the signal, recorded at a single wavelength, can be due to local changes of the shape of the CMS spectrum, induced by variations of the electronic environment of the states probed by charge at the interface with the dielectric.[44,45] It is therefore necessary to measure full local spectra in different regions of the CMS maps to verify whether spectral shifts from point to point in the accumulated channel could contribute to the observed texture.

Local CMS spectra were measured in two different domains (A and B in Figure 3a, left panel), with the same laser polarization. The dimensions of the probed spots depend on the wavelength and on the optics and approximately correspond to an area of $500 \times 500\ nm^2$ with the current setup. The CMS spectra normalized on the 690 nm main peak do not show any significant variation in shape (Figure 3b), and both spectra nicely follow the global CMS spectrum recorded macroscopically on the entire device (solid gray line) in a standard setup. Moreover, the local spectra do not show any significant spectral dependence with the laser polarization, as it can be seen from Figure 3c for two spectra collected at the same point with orthogonal polarizations. The small difference arising in the low-energy region of the spectra can be ascribed to slight misalignment of the TDMs of the two transitions peaking at 700 and 850 nm (*vide infra*).

We can therefore conclude that the observed modulation in the $\Delta T/T$ signal at 690 nm does not depend on local variation of the CMS spectrum. This observation is fundamental for the correct understanding of the dependence of the charge-induced spectral features on the microstructure of the semiconducting polymer within the channel.

From a more general point of view, it also evidences that the spectral broadening of the CMS bands observed when probing the channel in spots with lateral dimensions down to the resolution of the setup (~500 nm) corresponds to that recorded when probing the whole area of the device at once in a common CMS experiment (20 mm $\times$ 40 μm in this case).

p-CMM Mapping of Charge Absorption Features. To better characterize the relationship between the p-CMM signal and the electronic structure of the material, we have recorded maps at a wavelength corresponding to the absorption of the charged species (*i.e.*, $\lambda = 870$ nm). CMS maps collected in the same region at $\lambda = 690$ nm and $\lambda = 870$ nm are reported in Figure 3a. A comparison between the two clearly reveals that they present a very similar signal pattern. This comparison directly correlates the information about the TDM of two different electronic species, the first (at $\lambda = 690$ nm, left panel) being related to the transition of the neutral conjugated segments of P(NDI2OD-T2) and the second (at $\lambda = 870$ nm, right panel) to the charged (electron polaron) ones, providing an *experimental proof* that the

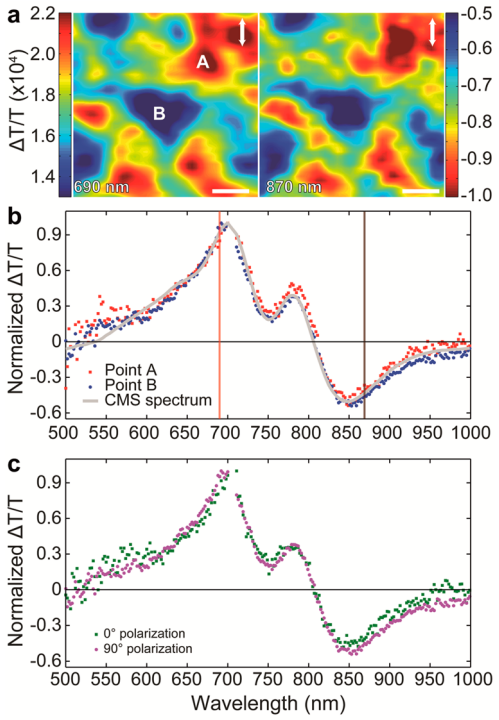

Figure 3. Spatial and polarization dependence of the local CMS spectra. (a) 5 × 5 μm^2 differential transmission maps recorded with polarized probe light at λ = 690 nm (left panel, bleaching peak, red line in panel b) and at λ = 870 nm (right panel, charge absorption peak, brown line in panel b). Scale bar is 1 μm. (b) Normalized local CMS spectra measured in the two different areas A and B at a fixed probe polarization, compared with the average CMS spectrum over the entire device recorded with a nonpolarized light probe. (c) Normalized local CMS spectra taken at the same point (B) with two orthogonal laser polarization. All spectra are normalized at the maximum of the main bleaching peak (*i.e.*, λ = 690 nm).

two TDMs oscillate mainly in the same direction. We can retrieve this information without relying on any assumption on the localization/delocalization of the charged states or on the local morphology, thus providing fundamental experimental information on the local spatial directionality of charge-induced transitions, not accessible in a working FET device with other available techniques.

Quantum-Chemical Calculations. To correlate these results with the actual film morphology, it is essential to know the relative orientation of the TDMs of both neutral and charged species with respect to the polymeric backbone. To access this level of insight, we have therefore performed quantum-chemical calculations (density functional theory, DFT, and time-dependent DFT, TD-DFT) for both the neutral and negatively charged (anion) species of P(NDI2OD-T2). A representative oligomer[46] of P(NDI2OD-T2) with four repeat units, (NDI2OD-T2)$_4$, has been described using the Coulomb attenuated method CAM-B3LYP[47] with double split Pope basis set 6-31G**; this level of theory has been shown to well describe the properties (localization, bond-length deformations, and reorganizational energy) in donor−acceptor copolymers.[46,48−50] More than 50 electronic states have been computed for both the neutral and the charged species at the TD-DFT level (full details about the computed electronic transitions are reported in the Supporting Information, Quantum Chemical Calculations). In Figure 4a,b the relevant molecular orbitals (MOs) involved in the main electronic transitions are displayed for both neutral and charged species.

For the case of the neutral P(NDI2OD-T2) chain segment, the main electronic transition is the $S_0 \rightarrow S_1$ (oscillator strength f = 1.57), and it can be described in the frame of one-particle transitions as a prevalent HOMO → LUMO, with also minor contributions from the HOMO−1 → LUMO+1 and HOMO → LUMO+2 orbitals (Figure 4a and Supporting Information). The nature of the MOs involved in the $S_0 \rightarrow S_1$ transition well reflects the donor−acceptor character of P(NDI2OD-T2), with the HOMOs being more localized on T2 units and LUMOs on NDI2OD ones.[46] The computed transition, related to the observed bleaching band in the CMS spectrum (λ = 690 nm), shows a TDM mainly directed *along* the polymer axis (Figure 4c, TDM_x = 12.37 D, TDM_y = 1.7 D, TDM_z = 0.07 D).

Excited-state TD-(U)DFT calculations have been carried out on the negatively charged (anion) species to assign the main absorption band in the CMS spectrum (Figure 3b). The band, located at 850 nm, can be assigned to the computed electronic transition, namely, the $S_0^- \rightarrow S_6^-$ (f = 0.50), with S_i^- being the ith electronic state of the negatively charged species. Assuming a one-particle description, the main single-occupied/unoccupied molecular orbitals (SOMOs and SUMOs) describing these transitions are reported in Figure 4b. SOMO-α is localized on the NDI2OD unit (being the electron acceptor moiety), whereas the single unoccupied orbitals involved are more delocalized over the entire donor−acceptor NDI2OD-T2 unit. The computed TDM components for the $S_0^- \rightarrow S_6^-$ transition are TDM_x = 8.32 D, TDM_y = 0.22 D, and TDM_z = 0.50 D. Similarly to what was obtained for the neutral species, the main electronic transition computed for the charged species is directed along the polymer axis (Figure 4c). From TDDFT calculations it can be predicted that the TDMs for the two probed transitions (neutral and charged species) are slightly misaligned by an angle of about 7°, which could cause the small differences in the low-energy regions of the spectra presented in Figure 3.

Here a question arises on the nature of the neutral and polaronic states probed by CMS in P(NDI2OD-T2) and if they can be properly described at an intramolecular level or whether they could show delocalization over adjacent conjugated segments.[51]

In order to exclude the possibility that eventual variations in molecular packing could have an effect on

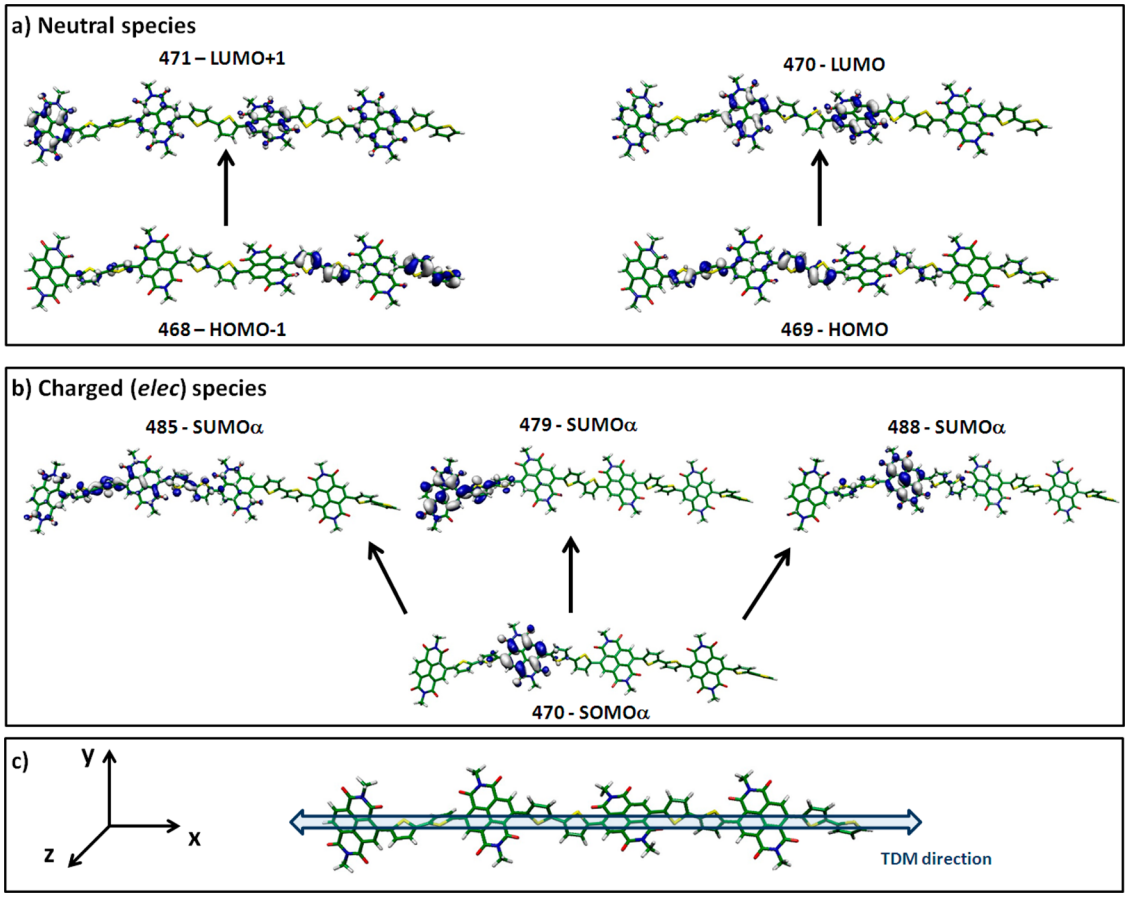

Figure 4. Quantum chemical calculations of the relevant transition dipole moments for the neutral and charged species of P(NDI2OD-T2). (a) TD-CAM-B3LYP/6-31G molecular orbitals involved in the $S_0 \rightarrow S_1$ transition for the neutral $(NDI2OD\text{-}T2)_4$ oligomer. (b) TD-(U)CAM-B3LYP/6-31G** molecular orbitals involved in the $S_0^- \rightarrow S_6^-$ transition for the charged $(NDI2OD\text{-}T2)_4$ oligomer (α indicates spin-up electron). (c) Sketch of a polymer fragment (alkyl chains omitted for clarity) with a reference Cartesian coordinate system and the direction (blue arrow) of the computed transition dipole moment for both the neutral and negatively charged species.**

TDM orientation with respect to the backbone, DFT calculations were performed on a cofacial dimer featuring two monomers of P(NDI2OD-T2) (Supporting Information, DFT/TDDFT calculation on a molecular dimer). The simulations confirm that the main electronic transitions computed on both the neutral and charged molecular aggregates show the same properties (in terms of state polarization and one-particle transitions) observed for the single oligomer. This evidence demonstrates that the electronic transitions probed have an intramolecular nature and confirms that the molecular packing has no significant effect on the TDMs' orientation.

Following the previous assignments, the CMS maps of the bleaching (at $\lambda = 690$ nm) and charge absorption (at $\lambda = 870$ nm) features (Figure 3) can be further rationalized and interpreted. On the basis of TD-DFT calculations, the experimentally probed TDMs can be used as a tool to investigate the *local* orientation of the P(NDI2OD-T2) backbones. In this framework CMS data can be used not only to study the electronic properties of the charge carrier but also to map the local morphology of the semiconducting film at the interface with the dielectric, and specifically of the fraction of polymeric segments involved in the charge transport. The CMS data can also be compared to the complementary information provided by OD maps, where *all* the bulk is probed, irrespectively of the involvement of the conjugated segments in the transport or not (*vide infra*).

Quantification of Local Orientational Order. Building on the knowledge of the TDM oscillation directions for the bleaching and absorption CMS features, we here make explicit use of the p-CMM technique to extract quantitative information on the orientational order of the polymeric backbones. To achieve this goal, we performed a numerical analysis of the maps of Figure 1 based on the method developed by Watts *et al.*[22] for transmission X-ray microscopy, modified to account for the different direction of the transition dipole moment of the optical absorption with respect to resonant soft X-ray measurements. Both OD and CMS maps were collected in the same $10 \times 10\ \mu m^2$ region at six different values of laser polarization θ (Supporting Information, Figures S5 and S6); the intensity data $I_{(x,y)}(\theta)$ for each pixel (x,y) were then fitted to the

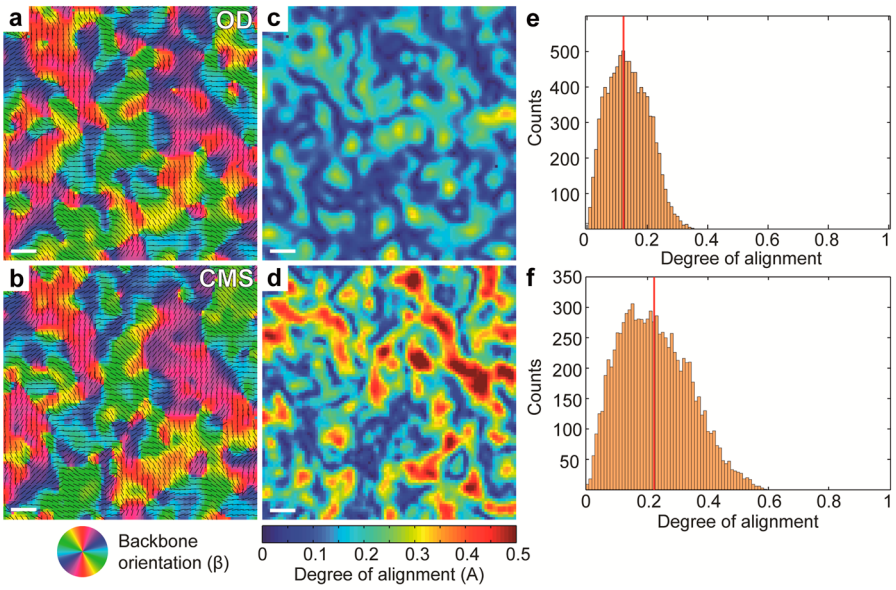

Figure 5. Quantitative analysis of the local alignment of polymeric backbones. (a, b) Local orientation of the aligned fraction of the polymeric backbones as calculated from the OD and CMS data, respectively. The analysis is performed on the same area of Figure 1. OD data (a) are sensitive to the entire bulk of the semiconducting layer, while the CMS signal (b) probes only the chain segments involved in the charge transport at the interface with the dielectric. (c, d) Local degree of alignment (*i.e.*, fraction of polymeric chains actually aligned along the preferential direction β), as calculated for OD and CMS maps, respectively. (e, f) Statistical distribution of the local degree of orientational order values for OD and CMS data reported in (c) and (d). The red line represents the mean value of the data.

expected cosine squared relation:

$$I_{(x,y)} = M_{(x,y)}\cos^2(\beta_{(x,y)} - \theta) + C_{(x,y)}$$

where $C_{(x,y)}$ is the fraction of the signal independent of the laser polarization, $M_{(x,y)}$ the amplitude of modulation, and $\beta_{(x,y)}$ the direction of preferential alignment of the polymeric backbones.

The extracted values for $\beta_{(x,y)}$ are reported in Figure 5a,b for the OD and CMS data, respectively (M and C maps can be found in Figure S7, Supporting Information). The angular maps report, for each point of the area probed in Figure 2, the local preferential alignment of the conjugated polymer segments. The two maps confirm that the local alignment of the backbones remains mainly the same going from the bulk of the semiconductor to the thin accumulation layer at the dielectric interface.

It is however important to note that only a fraction of the polymeric backbones are actually aligned along the retrieved directions, giving rise to the polarization-dependent part of the signal ($M_{(x,y)}$). The constant part ($C_{(x,y)}$) of the signal is related to the polymer fraction with no preferential alignment in the sample plane. From recent spectroscopic investigations on P(NDI2OD-T2) films, it has been shown that the P(NDI2OD-T2) backbones are mainly lying parallel to the sample plane.[53] In such a configuration the transition dipole moments, which are parallel to the polymer backbone, do not present any significant out-of-plane projection. On this basis, quantitative information on the fraction of aligned molecules can be derived, for each pixel of the maps, as

$$A_{(x,y)} = \frac{M_{(x,y)}}{M_{(x,y)} + 2C_{(x,y)}}$$

where the factor 2 takes into account the fact that each segment of the not-aligned fraction, due to the TDM anisotropy, has a halved probability, on average, to absorb a photon. The resulting maps for the local degree of chain alignment ($A_{(x,y)}$) are given in Figure 5c, d for the OD and CMS data, respectively. From the OD image, which is related to the bulk morphology of the semiconducting film, we observe that a very scarce fraction of chains are aligned, between 5% and 30% (the statistical distribution of the data is reported in Figure 5e). On the other side, the data extracted from the CMS maps give clear evidence that the actual polymer segments visited by the charge possess an increased degree of orientational order, with values up to more than 50% (Figure 5f and Figure S8, Supporting Information). Either the polymer chains within the thin accumulation layer show a higher degree of orientational order, which is partially lost in the whole bulk of the film, or charge preferably selects more oriented domains in their percolation path. It is worth noting that the calculated data for the degree of alignment can be considered as lower limits, especially at the domain boundaries, because of the finite size of the probing laser spot (~500 nm) that can mediate signals from regions with different orientations.

P(NDI2OD-T2) Device with Enhanced Electron Mobility. To fully show the potential of the p-CMM technique, we

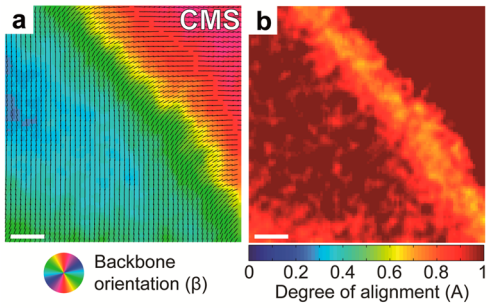

Figure 6. p-CMM data analysis for a toluene-cast P(NDI2OD-T2) device. (a) Local orientation of the aligned fraction of the polymeric backbones as calculated from the CMS data for a device with the semiconducting P(NDI2OD-T2) layer cast from a toluene solution. The map is a 35 × 35 μm^2 region inside the channel of the device. (b) Local degree of alignment relative to the map of panel (a). Scale bar is 5 μm.

analyzed a P(NDI2OD-T2) transistor in which the semiconducting layer was cast from a toluene solution, yielding a long-range order film with improved electron mobility. We have in fact recently shown that by spinning solutions of P(NDI2OD-T2) rich in aggregates, as induced by toluene,[52] it is possible to obtain birefringent films, with well-oriented domains extending up to hundreds of micrometers.[27] FETs based on these highly oriented films were demonstrated to have a strongly improved electron saturation mobility, exceeding 1 $cm^2/(V\ s)$, as compared to 0.1−0.3 $cm^2/(V\ s)$ recorded in the case of dichlorobenzene with the same polymer dielectric (Figure S2, Supporting Information). The results of the analysis for the CMS data collected on a 35 × 35 μm^2 area on a device with P(NDI2OD-T2) processed from toluene are reported in Figure 6 (CMS data and the complete results of the analysis are shown in Figures S10 and S11, Supporting Information).

The angular map (Figure 6a) evidences that charge resides on domains of aligned polymer segments that span several tens of micrometers. In particular, it is possible to observe two distinct domains with orthogonal angular alignment of the backbones (the green and the red regions); the transition between the two domains however is not abrupt, but occurs smoothly in 5−10 μm (blue region), well in agreement with the morphological analysis reported in ref 27. Even more strikingly, the degree of alignment (Figure 6b) is extremely high and very close to 100% in the two domains, with only a small decrease in the transition region, where in any case it remains above 60%.

DISCUSSION

We have adopted p-CMM to map the polarization-dependent charged-induced features within the accumulated channel of high-mobility, solution-processed polymer field-effect transistors. Being a noninvasive technique, the measurements can be performed *in situ* in actual working devices, therefore investigating the real interface between the semiconductor and dielectric, whose energetic, morphology, and physical extension may be largely affected by the chosen dielectric and its solvent.[32,33,54] Charge is accumulated and modulated within the channel, and spectral features of the conjugated segments they visit are measured. In this way we can retrieve specific information on the sites actually involved in charge transport, which account for less than 1% of all available sites within the nanometer thick channel, at typical densities achieved in OFETs. The control of the polarization and the possibility to measure at different energies enable the unveiling of domains with different preferential alignment of charge-induced TDMs, supported by the fact that the shape of full local charge-induced spectra is constant over the channel area and independent of the polarization. In combination with quantum-chemical calculations, performed to assign the probed electronic transitions and determine the oscillation direction of TDM with respect to the polymer backbone, we gain also access the local direction and degree of preferential alignment of the charge-probed polymeric backbones. In p-CMM, charge is the actual probe that reveals the morphological features of those structural domains that are relevant to define mobility. In fact, only mobile charges are capable of following the modulation signal and are thus the ones that determine the channel current, from which the mobility is estimated.

The results reported for FETs based on P(NDI2OD-T2) clearly demonstrate the importance of having selective access to the sites probed by charge in order to correctly investigate the structure−properties relationship in the material. This aspect is evidenced by the comparison with the simultaneously recorded OD data, where all molecules in the bulk of the film are probed instead (upper panels of Figure 5). On one hand, we can directly verify that there is agreement in size and preferred directionality of structural domains within the bulk and charge-probed domains in the channel. On the other, in the p-CMM maps we evidence a marked increase of alignment in the charge-probed interfacial region with respect to the bulk probed by the OD maps (Figure 5). This effect could be partially related to the fact that throughout the ∼40 nm thickness of the film there is a greater probability for the polymer chains to misalign with respect to each other, compared to the few nanometers thin accumulation layer. However, the observation that the angular maps for the two cases are almost identical is a hint that the structural properties of the material are maintained throughout the entire thickness of the semiconducting layer. Since what we are mapping with p-CMM is the morphology of the portion of the device involved in charge transport, the improved degree of alignment in p-CMM maps is an indication that more orientationally ordered domains offer the possibility to find energetically favorable sites for charge.[1,21,55,56]

The limitation of the p-CMM technique resides in its spatial resolution, which is determined by diffraction. With our current setup and in the investigated spectral range we have a resolution of approximately 500 nm. On one hand this resolution can be further improved by probing the samples at higher energies and by benefiting from higher numerical aperture objectives. On the other hand, the importance of this work is also to clarify that the scale length accessible with p-CMM is relevant for the study of charge transport in high-mobility polymer semiconductors. Indeed, the effect on transport properties of the extension of charge-probed orientational domains and of the degree of order within them emerges by comparing maps on P(NDI2OD-T2) films deposited from dichlorobenzene ($\mu \approx 0.1$ cm^2/(V s)) and from toluene ($\mu \approx 0.8$ cm^2/(V s)) (Figures 5, 6). In the lower mobility dichlorobenzene spin-cast films, charge flowing from source to drain probes domains indifferently displaying all orientations, having less degree of order and being smaller in extent (up to a few micrometers). Instead, in the case of the high-mobility toluene spin-cast films, charge is transported through domains with only two preferential orientations, one orthogonal to the other, both extending long enough to bridge source and drain contacts. Moreover, in the wider domains, conjugated segments probed by charge are almost perfectly aligned. Together with the fact that we are in the presence of localized charge, these observations clarify that an orientational order capable of providing an efficient pathway for charge percolation over a distance comparable to the channel length can strongly improve the measured field-effect mobility.

In addition, if charge shows polaronic effects, as in the case of organic semiconductors, p-CMM offers the possibility to specifically probe and compare the relative orientation of the dipole moments of different charge-induced transitions in a semiconducting film without the need of any assumption on their nature or spatial extension. We have shown in the case of P(NDI2OD-T2), irrespectively of the intra- or intermolecular nature of the polarons, the TDMs of the neutral ($\lambda = 690$ nm) and charged ($\lambda = 870$ nm) species oscillate essentially in the same direction, an observation that has been corroborated by DFT and TD-DFT calculations.

CONCLUSION

In conclusion, the possibility to investigate at the same time the electronic properties (CMS) and the local degree of order of the only polymer chains contributing to charge transport in the accumulated channel of a FET device makes p-CMM a unique, yet simple and very accessible, tool to study structure−property relationships in organic semiconductors with an unprecedented selectivity on the film region relevant for charge transport phenomena. p-CMM therefore offers the potential to fill the still existing gap between morphological structures of organic thin films and how charge is accumulated and distributed within them.

METHODS

Device Fabrication and Electrical Characterization. Thoroughly cleaned 1737F glass was used as a substrate for all the films realized in this work. FETs were fabricated according to a top-gate, bottom-contact architecture. Bottom Au contacts were defined by a lift-off photolithographic process with a 0.7 nm thick Cr adhesion layer. The thickness of the Au contacts was 30 nm. Source and drain electrodes with a channel width (W) of 20 mm and length (L) of 40 μm have been realized. Patterned substrates were cleaned in a sonic bath in isopropyl alcohol for 2−3 min before deposition of the semiconductor or the dielectric. P(NDI2OD-T2) was purchased from Polyera Corporation (Activink N2200). Solutions of P(NDI2OD-T2) in toluene (5 g/L) and DCB (9 g/L) were prepared, filtered, and deposited by spin-coating at 1000 rpm for 30 s in the case of toluene and 90 s in the case of DCB in a nitrogen glovebox. The semiconductor was then annealed for 14 h at 120 °C on a hot plate in a nitrogen atmosphere. Topography and polarized microscopy images of the polymer thin films have been previously reported.[27] As the dielectric layer, the perfluorinated polymer CYTOP CTL-809 M dielectric (Asahi Glass) was spun as received at 6000 rpm for 90 s (film thickness ~550 nm); thermally evaporated 4.5 nm thick Au transparent gate electrodes were employed.

The electrical characteristics of transistors were measured in a nitrogen glovebox on a Wentworth Laboratories probe station with an Agilent B1500A semiconductor device analyzer. Saturation charge carrier mobility values were extracted by the transfer characteristic curves according to the gradual channel approximation,[57] following the expression $I_d = \mu_{sat} \times C_{die} \times W/2L \times (V_g - V_t)^2$, where I_d is the drain current, μ_{sat} is the saturation mobility, C_{die} is the specific dielectric capacitance, W and L are the width and the length of the channel, respectively, V_g is the gate voltage, V_d is the drain voltage, and V_t is the threshold voltage. Accordingly, the V_g-dependent values of μ_{sat} were obtained from the slope of $I_d^{0.5}$ *versus* V_g, calculated every three points around each V_g value.

Charge Modulation Microscopy. The CMM data were collected with a homemade confocal microscope in transmission configuration. The light source consisted of a supercontinuum laser (NKT Photonics, SuperK Extreme) monochromated by an acousto-optic modulator (NKT Photonics, SuperK Select) in the 500−1000 nm region with line widths between 2 and 5 nm. The polarization of the laser was then controlled with a half-wave plate and a linear polarizer. The light was then focused on the sample with a 0.7 N.A. objective (S Plan Fluor 60×, Nikon) and collected by a second 0.75 N.A. objective (CFI Plan Apochromat VC 20×, Nikon). The collected light was focused on the entrance of a multimodal glass fiber with a 50 μm core, acting as confocal aperture and revealed by a silicon photodetector (FDS100, Thorlabs). The signal was amplified by a transimpedance amplifier (DHPCA-100, Femto) and supplied both to a DAQ (to record the transmission signal, T) and to a lock-in amplifier (SR830 DSP, Stanford Research Systems) to retrieve the differential transmission data, ΔT. All data were collected by a custom Labview Software that also controlled the raster scan of the sample *via* a 3D piezo stage (P-517, Physik Instrumente) and the laser system. The OD values were obtained from T as described in the Supplementary Discussion, while the CMS data were calculated as $\Delta T/T$.

The sample was kept in an inert atmosphere by fluxing nitrogen in a homemade chamber. The gate voltage of the transistor was sinusoidally modulated at 989 Hz between 20 and

60 V (unless specified otherwise) with a waveform generator (3390, Keithley) amplified by a high-voltage amplifier (WMA-300, Falco Systems), while the source and drain contacts were kept at short-circuit. Signal maps were collected by raster scanning the sample at 250 ms per pixel, with a lock-in integration time of 100 ms. All data were processed with Matlab. OD and CMS images were smoothed by convolution with a bell-shaped function.

Quantum Chemical Calculations. P(NDI2OD-T2) has been modeled by using an oligomer approach. To describe correctly the electronic structure properties, we used an oligomer length of four units, $(NDI2OD\text{-}T2)_4$. The Coulomb attenuated method CAM-B3LYP functional coupled with a double split Pope basis set, 6-31G**, has been used with the restricted and unrestricted (U) wave functions for the neutral and charged species, respectively. Spin contamination has been evaluated as $\langle S \rangle = 0.77$ for the negatively charged species. TD-(U)CAM-B3LYP/6-31G** calculations have been carried out considering up to 50 excited states for both neutral and charged species. The Gaussian09 package[58] has been used for all the quantum-chemical calculations. To investigate possible effects of the polymer packing on the electronic transitions, the monomer ($n = 1$) of P(NDI2OD-T2) has been considered. The dimer, *i.e.*, two cofacial monomers, has been fully optimized in the neutral and charged state by using the (U)M06-2X/6-311G** level of theory. The electronic transitions for both neutral and charged dimers have been computed at the TD-(U)CAM-B3LYP/6-31G** level. In the Supporting Information are reported the details of these calculations. In the spectral region of interest (main electronic transition with high oscillator strength) no differences have been computed between the neutral and the charged cofacial dimer, thus excluding some effect induced by the aggregation, at least on the CMS band peaked at $\lambda = 850$ nm.

Conflict of Interest: The authors declare no competing financial interest.

Supporting Information Available: Supplementary discussion about the charge density estimation; signals measured by p-CMM; optical density maps; CMS of P(NDI2OD-T2); quantum-chemical calculations; DFT/TDDFT calculation on a molecular dimer. Supplementary figures: experimental setup; device scheme and electrical characteristics; OD spectrum of P(NDI2OD-T2); p-CMM signal frequency dependence; angular dependence of OD and CMS maps; results of quantitative analysis of p-CMM maps; stability of device during measurement. This material is available free of charge *via* the Internet at http://pubs.acs.org.

Acknowledgment. M.C. acknowledges financial support from Fondazione Cariplo under project Indixi, Grant No. 2011-0368, and from the European Union through the Marie-Curie Career Integration Grant 2011 "IPPIA", within the EU Seventh Framework Programme (FP7/2007−2013) under grant agreement No. PCIG09-GA-2011-291844. The authors are thankful to V. D'Innocenzo and A. Petrozza for useful discussions on charge modulation microscopy and to S. Perissinotto for help in measuring optical density spectra.

REFERENCES AND NOTES

1. Rivnay, J.; Mannsfeld, S.; Miller, C.; Salleo, A.; Toney, M. Quantitative Determination of Organic Semiconductor Microstructure from the Molecular to Device Scale. *Chem. Rev.* **2012**, *112*, 5488–5519.
2. Noriega, R.; Rivnay, J.; Vandewal, K.; Koch, F.; Stingelin, N.; Smith, P.; Toney, M.; Salleo, A. A General Relationship between Disorder, Aggregation and Charge Transport in Conjugated Polymers. *Nat. Mater.* **2013**, *12*, 1038–1044.
3. Takacs, C.; Treat, N.; Krämer, S.; Chen, Z.; Facchetti, A.; Chabinyc, M.; Heeger, A. Remarkable Order of a High-Performance Polymer. *Nano Lett.* **2013**, *13*, 2522–2527.
4. Bräuer, B.; Virkar, A.; Mannsfeld, S. C. B.; Bernstein, D. P.; Kukreja, R.; Chou, K. W.; Tyliszczak, T.; Bao, Z.; Acremann, Y. X-Ray Microscopy Imaging of the Grain Orientation in a Pentacene Field-Effect Transistor. *Chem. Mater.* **2010**, *22*, 3693–3697.
5. Gargi, D.; Kline, R. J.; DeLongchamp, D. M.; Fischer, D. A.; Toney, M. F.; O'Connor, B. T. Charge Transport in Highly Face-On Poly(3-Hexylthiophene) Films. *J. Phys. Chem. C* **2013**, *117*, 17421–17428.
6. Li, J.; Zhao, Y.; Tan, H.; Guo, Y.; Di, C.-A.; Yu, G.; Liu, Y.; Lin, M.; Lim, S.; Zhou, Y.; *et al*. A Stable Solution-Processed Polymer Semiconductor with Record High-Mobility for Printed Transistors. *Sci. Rep.* **2012**, *2*, 754.
7. Kang, I.; An, T.; Hong, J.; Yun, H.-J.; Kim, R.; Chung, D.; Park, C.; Kim, Y.-H.; Kwon, S.-K. Effect of Selenophene in a DPP Copolymer Incorporating a Vinyl Group for High-Performance Organic Field-Effect Transistors. *Adv. Mater.* **2013**, *25*, 524–528.
8. Chen, Z.; Lee, M.; Shahid Ashraf, R.; Gu, Y.; Albert-Seifried, S.; Meedom Nielsen, M.; Schroeder, B.; Anthopoulos, T.; Heeney, M.; McCulloch, I.; *et al*. High-Performance Ambipolar Diketopyrrolopyrrole-Thieno[3,2-b]thiophene Copolymer Field-Effect Transistors with Balanced Hole and Electron Mobilities. *Adv. Mater.* **2012**, *24*, 647–652.
9. Lee, J.; Han, A.-R.; Yu, H.; Shin, T.; Yang, C.; Oh, J. Boosting the Ambipolar Performance of Solution-Processable Polymer Semiconductors *via* Hybrid Side-Chain Engineering. *J. Am. Chem. Soc.* **2013**, *135*, 9540–9547.
10. Kim, R.; Amegadze, P. S. K.; Kang, I.; Yun, H.-J.; Noh, Y.-Y.; Kwon, S.-K.; Kim, Y.-H. High-Mobility Air-Stable Naphthalene Diimide-Based Copolymer Containing Extended π-Conjugation for n-Channel Organic Field Effect Transistors. *Adv. Funct. Mater.* **2013**, *23*, 5719–5727.
11. Baeg, K.-J.; Caironi, M.; Noh, Y.-Y. Toward Printed Integrated Circuits Based on Unipolar or Ambipolar Polymer Semiconductors. *Adv. Mater.* **2013**, *25*, 4210–4244.
12. Gelinck, G.; Heremans, P.; Nomoto, K.; Anthopoulos, T. Organic Transistors in Optical Displays and Microelectronic Applications. *Adv. Mater.* **2010**, *22*, 3778–3798.
13. Street, R.; Northrup, J.; Salleo, A. Transport in Polycrystalline Polymer Thin-Film Transistors. *Phys. Rev. B* **2005**, *71*, 165202.
14. Sirringhaus, H.; Brown, P. J.; Friend, R. H.; Nielsen, M. M.; Bechgaard, K.; Langeveld-Voss, B. M. W.; Spiering, A. J. H.; Janssen, R. A. J.; Meijer, E. W.; Herwig, P.; *et al*. Two-Dimensional Charge Transport in Self-Organized, High-Mobility Conjugated Polymers. *Nature* **1999**, *401*, 685–688.
15. McCulloch, I.; Heeney, M.; Bailey, C.; Genevicius, K.; Macdonald, I.; Shkunov, M.; Sparrowe, D.; Tierney, S.; Wagner, R.; Zhang, W.; *et al*. Liquid-Crystalline Semiconducting Polymers with High Charge-Carrier Mobility. *Nat. Mater.* **2006**, *5*, 328–333.
16. Yan, H.; Chen, Z.; Zheng, Y.; Newman, C.; Quinn, J.; Dötz, F.; Kastler, M.; Facchetti, A. A High-Mobility Electron-Transporting Polymer for Printed Transistors. *Nature* **2009**, *457*, 679–686.
17. Chen, Z.; Zheng, Y.; Yan, H.; Facchetti, A. Naphthalenedicarboximide- vs Perylenedicarboximide-Based Copolymers. Synthesis and Semiconducting Properties in Bottom-Gate N-Channel Organic Transistors. *J. Am. Chem. Soc.* **2009**, *131*, 8–9.
18. Luzio, A.; Fazzi, D.; Natali, D.; Giussani, E.; Baeg, K. J.; Chen, Z.; Noh, Y. Y.; Facchetti, A.; Caironi, M. Synthesis, Electronic Structure, and Charge Transport Characteristics of Naphthalenediimide Based Co-Polymers with Different Oligothiophene Donor Units. *Adv. Funct. Mater.* **2013**, *24*, 1151–1162.
19. Zhang, X.; Richter, L.; DeLongchamp, D.; Kline, R.; Hammond, M.; McCulloch, I.; Heeney, M.; Ashraf, R.; Smith, J.; Anthopoulos, T.; *et al*. Molecular Packing of High-Mobility Diketo Pyrrolo-Pyrrole Polymer Semiconductors with Branched Alkyl Side Chains. *J. Am. Chem. Soc.* **2011**, *133*, 15073–15084.
20. Zhang, W.; Smith, J.; Watkins, S.; Gysel, R.; McGehee, M.; Salleo, A.; Kirkpatrick, J.; Ashraf, S.; Anthopoulos, T.; Heeney, M.; *et al*. Indacenodithiophene Semiconducting Polymers for High-Performance, Air-Stable Transistors. *J. Am. Chem. Soc.* **2010**, *132*, 11437–11439.
21. Zhang, X.; Bronstein, H.; Kronemeijer, A.; Smith, J.; Kim, Y.; Kline, R.; Richter, L.; Anthopoulos, T.; Sirringhaus, H.; Song,

K.; *et al*. Molecular Origin of High Field-Effect Mobility in an Indacenodithiophene-Benzothiadiazole Copolymer. *Nat. Commun.* **2013**, *4*, 2238.
22. Watts, B.; Schuettfort, T.; McNeill, C. R. Mapping of Domain Orientation and Molecular Order in Polycrystalline Semiconducting Polymer Films with Soft X-Ray Microscopy. *Adv. Funct. Mater.* **2011**, *21*, 1122–1131.
23. Schuettfort, T.; Watts, B.; Thomsen, L.; Lee, M.; Sirringhaus, H.; McNeill, C. Microstructure of Polycrystalline PBTTT Films: Domain Mapping and Structure Formation. *ACS Nano* **2012**, *6*, 1849–1864.
24. Collins, B.; Cochran, J.; Yan, H.; Gann, E.; Hub, C.; Fink, R.; Wang, C.; Schuettfort, T.; McNeill, C.; Chabinyc, M.; *et al.* Polarized X-Ray Scattering Reveals Non-Crystalline Orientational Ordering in Organic Films. *Nat. Mater.* **2012**, *11*, 536–543.
25. Street, R. Materials Science. Unraveling Charge Transport in Conjugated Polymers. *Science* **2013**, *341*, 1072–1073.
26. Kim, B.-G.; Jeong, E.; Chung, J.; Seo, S.; Koo, B.; Kim, J. A Molecular Design Principle of Lyotropic Liquid-Crystalline Conjugated Polymers with Directed Alignment Capability for Plastic Electronics. *Nat. Mater.* **2013**, *12*, 659–664.
27. Luzio, A.; Criante, L.; D'Innocenzo, V.; Caironi, M. Control of Charge Transport in a Semiconducting Copolymer by Solvent-Induced Long-Range Order. *Sci. Rep.* **2013**, *3*, 3425.
28. Kuehn, S.; Pingel, P.; Breusing, M.; Fischer, T.; Stumpe, J.; Neher, D.; Elsaesser, T. High-Resolution Near-Field Optical Investigation of Crystalline Domains in Oligomeric PQT-12 Thin Films. *Adv. Funct. Mater.* **2011**, *21*, 860–868.
29. Rivnay, J.; Jimison, L.; Northrup, J.; Toney, M.; Noriega, R.; Lu, S.; Marks, T.; Facchetti, A.; Salleo, A. Large Modulation of Carrier Transport by Grain-Boundary Molecular Packing and Microstructure in Organic Thin Films. *Nat. Mater.* **2009**, *8*, 952–958.
30. Watts, B.; McNeill, C. Simultaneous Surface and Bulk Imaging of Polymer Blends with X-Ray Spectromicroscopy. *Macromol. Rapid Commun.* **2010**, *31*, 1706–1712.
31. Schuettfort, T.; Thomsen, L.; McNeill, C. Observation of a Distinct Surface Molecular Orientation in Films of a High Mobility Conjugated Polymer. *J. Am. Chem. Soc.* **2013**, *135*, 1092–1101.
32. Li, J.; Du, J.; Xu, J.; Chan, H. L.; Yan, F. The Influence of Gate Dielectrics on a High-Mobility N-Type Conjugated Polymer in Organic Thin-Film Transistors. *Appl. Phys. Lett.* **2012**, *100*, 033301.
33. Baeg, K.-J.; Facchetti, A.; Noh, Y.-Y. Effects of Gate Dielectrics and Their Solvents on Characteristics of Solution-Processed N-Channel Polymer Field-Effect Transistors. *J. Mater. Chem.* **2012**, *22*, 21138–21143.
34. Yan, H.; Schuettfort, T.; Kronemeijer, A. J.; McNeill, C. R.; Ade, H. W. Influence of Dielectric-Dependent Interfacial Widths on Device Performance in Top-Gate P(NDI2OD-T2) Field-Effect Transistors. *Appl. Phys. Lett.* **2012**, *101*, 093308.
35. Tanase, C.; Meijer, E. J.; Blom, P. W. M.; de Leeuw, D. M. Unification of the Hole Transport in Polymeric Field-Effect Transistors and Light-Emitting Diodes. *Phys. Rev. Lett.* **2003**, *91*, 216601.
36. Coehoorn, R.; Pasveer, W. F.; Bobbert, P. A.; Michels, M. A. J. Charge-Carrier Concentration Dependence of the Hopping Mobility in Organic Materials with Gaussian Disorder. *Phys. Rev. B* **2005**, *72*, 155206.
37. Celebrano, M.; Sciascia, C.; Cerullo, G.; Zavelani-Rossi, M.; Lanzani, G.; Cabanillas-Gonzalez, J. Imaging the Electric-Field Distribution in Organic Devices by Confocal Electroreflectance Microscopy. *Adv. Funct. Mater.* **2009**, *19*, 1180–1185.
38. Sciascia, C.; Celebrano, M.; Binda, M.; Natali, D.; Lanzani, G.; Cabanillas-Gonzalez, J. R. Electric Field and Charge Distribution Imaging with Sub-Micron Resolution in an Organic Thin-Film Transistor. *Org. Electron.* **2012**, *13*, 66–70.
39. Brown, P. J.; Sirringhaus, H.; Harrison, M.; Shkunov, M.; Friend, R. H. Optical Spectroscopy of Field-Induced Charge in Self-Organized High Mobility Poly (3-Hexylthiophene). *Phys. Rev. B* **2001**, *63*, 125204.
40. Chen, Z.; Bird, M.; Lemaur, V.; Radtke, G.; Cornil, J.; Heeney, M.; McCulloch, I.; Sirringhaus, H. Origin of the Different Transport Properties of Electron and Hole Polarons in an Ambipolar Polyselenophene-Based Conjugated Polymer. *Phys. Rev. B* **2011**, *84*, 115211.
41. Xu, H.; Jiang, Y.; Li, J.; Ong, B. S.; Shuai, Z.; Xu, J.; Zhao, N. Spectroscopic Study of Electron and Hole Polarons in a High-Mobility Donor–Acceptor Conjugated Copolymer. *J. Phys. Chem. C* **2013**, *117*, 6835–6841.
42. Sciascia, C.; Martino, N.; Schuettfort, T.; Watts, B.; Grancini, G.; Antognazza, M.; Zavelani-Rossi, M.; McNeill, C.; Caironi, M. Sub-Micrometer Charge Modulation Microscopy of a High Mobility Polymeric N-Channel Field-Effect Transistor. *Adv. Mater.* **2011**, *23*, 5086–5090.
43. Harima, Y.; Ishiguro, Y.; Komaguchi, K.; Imae, I.; Ooyama, Y. Optical Absorption Spectrum of Pentacene Cation Radicals Measured by Charge-Modulation Spectroscopy. *Chem. Phys. Lett.* **2010**, *495*, 228–231.
44. Caironi, M.; Bird, M.; Fazzi, D.; Chen, Z.; Pietro, R. D.; Newman, C.; Facchetti, A.; Sirringhaus, H. Very Low Degree of Energetic Disorder as the Origin of High Mobility in an N-Channel Polymer Semiconductor. *Adv. Funct. Mater.* **2011**, *21*, 3371–3381.
45. Lee, M. J.; Chen, Z.; Pietro, R.; di Heeney, M.; Sirringhaus, H. Electrooptical Spectroscopy of Uniaxially Aligned Polythiophene Films in Field-Effect Transistors. *Chem. Mater.* **2013**, *25*, 2075–2082.
46. Fazzi, D.; Caironi, M.; Castiglioni, C. Quantum-Chemical Insights into the Prediction of Charge Transport Parameters for a Naphthalenetetracarboxydiimide-Based Copolymer with Enhanced Electron Mobility. *J. Am. Chem. Soc.* **2011**, *133*, 19056–19059.
47. Yanai, T.; Tew, D.; Handy, N. A New Hybrid Exchange–Correlation Functional Using the Coulomb-Attenuating Method (CAM-B3LYP). *Chem. Phys. Lett.* **2004**, *393*, 51–57.
48. Wiebeler, C.; Tautz, R.; Feldmann, J.; Hauff, E.; von Como, E.; Da Schumacher, S. Spectral Signatures of Polarons in Conjugated Co-Polymers. *J. Phys. Chem. B* **2012**, *117*, 4454–4460.
49. Nayyar, I. H.; Batista, E. R.; Tretiak, S.; Saxena, A.; Smith, D. L.; Martin, R. L. Localization of Electronic Excitations in Conjugated Polymers Studied by DFT. *J. Phys. Chem. Lett.* **2011**, *2*, 566–571.
50. Nayyar, I. H.; Batista, E. R.; Tretiak, S.; Saxena, A.; Smith, D. L.; Martin, R. L. Role of Geometric Distortion and Polarization in Localizing Electronic Excitations in Conjugated Polymers. *J. Chem. Theory Comput.* **2013**, *9*, 1144–1154.
51. Beljonne, D.; Cornil, J.; Sirringhaus, H.; Brown, P. J.; Shkunov, M.; Friend, R. H.; Brédas, J.-L. Optical Signature of Delocalized Polarons in Conjugated Polymers. *Adv. Funct. Mater.* **2001**, *11*, 229–234.
52. Steyrleuthner, R.; Schubert, M.; Howard, I.; Klaumünzer, B.; Schilling, K.; Chen, Z.; Saalfrank, P.; Laquai, F.; Facchetti, A.; Neher, D. Aggregation in a High-Mobility N-Type Low-Bandgap Copolymer with Implications on Semicrystalline Morphology. *J. Am. Chem. Soc.* **2012**, *134*, 18303–18317.
53. Giussani, E.; Fazzi, D.; Brambilla, L.; Caironi, M.; Castiglioni, C. Molecular Level Investigation of the Film Structure of a High Electron Mobility Copolymer *via* Vibrational Spectroscopy. *Macromolecules* **2013**, *46*, 2658–2670.
54. Yan, H.; Wang, C.; Garcia, A.; Swaraj, S.; Gu, Z.; McNeill, C. R.; Schuettfort, T.; Sohn, K. E.; Kramer, E. J.; Bazan, G. C. Interfaces in Organic Devices Studied with Resonant Soft X-Ray Reflectivity. *J. Appl. Phys.* **2011**, *110*, 102220.
55. Vehoff, T.; Baumeier, B.; Troisi, A.; Andrienko, D. Charge Transport in Organic Crystals: Role of Disorder and Topological Connectivity. *J. Am. Chem. Soc.* **2010**, *132*, 11702–11708.
56. McMahon, D. P.; Cheung, D. L.; Goris, L.; Dacuña, J.; Salleo, A.; Troisi, A. Relation between Microstructure and Charge Transport in Polymers of Different Regioregularity. *J. Phys. Chem. C* **2011**, *115*, 19386–19393.
57. Sze, S. M.; Ng, K. K. *Physics of Semiconductor Devices*, 3rd ed.; John Wiley & Sons, Inc: New York, 2006.
58. Frisch, M. J.; Trucks, G. W.; Schlegel, H. B.; Scuseria, G. E.; Robb, M. A.; Cheeseman, J. R.; Scalmani, G.; Barone, V.; Mennucci, B.; Petersson, G. A.; *et al. Gaussian 09*, Revision A.1; Gaussian, Inc.: Wallingford, CT, 2009.